Chadwick Austin, J (Orcid ID: 0000-0002-2552-0083)
Lamb Michael, P (Orcid ID: 0000-0002-5701-0504)
Moodie Andrew, J. (Orcid ID: 0000-0002-6745-036X)
Parker Gary (Orcid ID: 0000-0001-5973-5296)
Nittrouer Jeffrey, Albert (Orcid ID: 0000-0002-4762-0157)

Origin of a preferential avulsion node on lowland river deltas

A. J. Chadwick[1*], M. P. Lamb[1], A.J. Moodie[2], G. Parker[3], J.A. Nittrouer[2]

[1]Division of Geological and Planetary Sciences, California Institute of Technology, 1200 E. California Boulevard, Pasadena, California 91125, USA

[2]Department of Earth, Environmental and Planetary Science, Rice University, Houston, Texas, USA

[3]Department of Civil and Environmental Engineering and Department of Geology, University of Illinois at Urbana-Champaign, Urbana, IL, USA

*Corresponding author: Austin Chadwick (achadwick@caltech.edu)

This article has been accepted for publication and undergone full peer review but has not been through the copyediting, typesetting, pagination and proofreading process which may lead to differences between this version and the Version of Record. Please cite this article as doi: 10.1029/2019GL082491

Abstract

River deltas are built by cycles of lobe growth and abrupt channel shifts, or avulsions, that occur within the backwater zone of coastal rivers. Previous numerical models differ on the origin of backwater-scaled avulsion nodes, and their consistency with experimental data. To unify previous work, we developed a numerical model of delta growth that includes backwater hydrodynamics, river-mouth progradation, relative sea-level rise, variable flow regimes, and cycles of lobe growth, abandonment, and reoccupation. For parameter space applicable to lowland deltas, we found that flow variability is the primary mechanism to cause persistent avulsion nodes by focusing aggradation within the backwater zone. Backwater-scaled avulsion nodes also occur under less likely scenarios of initially uniform bed slopes, or during rapid relative sea-level rise and marine transgression. Our findings suggest that flow variability is a fundamental control on long-term delta morphodynamics.

Key Points:

- Rivers on lowland deltas have repeated avulsions at a preferential location at the delta apex that scales with the backwater length.
- A preferential avulsion node occurs due to flow variability that focuses bed aggradation in the backwater zone.
- A preferential node under constant discharge simulations in previous work resulted from assumed initial conditions of uniform bed slope.

Plain Language Summary

River deltas are important for farming and drinking water, human populations, and diverse wildlife. Rivers on deltas are unstable and abruptly change course every 10-1000 years. These channel shifts are necessary for sustaining coastal landscapes, but also pose significant hazards. Here we present a mathematical model that shows how rivers require occasional floods, similar to what is observed on natural rivers, to give rise to a predictable location where rivers shift their course. Model simulations without floods produce rivers that change course at random locations, unlike natural rivers. Our findings resolve differences in previous studies about the importance of floods, and illustrate that occasional floods are necessary for natural delta growth.

1. Introduction

Many deltas are built through the deposition of discrete lobes punctuated by river avulsions, or channel-switching events (Slingerland & Smith, 2004; Jerolmack, 2009). River avulsions pose a hazard to human life and property (Soong & Zhao, 1994; Kidder & Liu, 2017) and are fundamental for building new land and nourishing wetland ecosystems (Richards et al., 2002; Edmonds et al., 2009). We need to understand where avulsions occur on lowland deltas to improve predictions of flooding hazards and sustainability.

Deltaic avulsions tend to occur repeatedly at a similar location, termed the avulsion node, which sets the delta-apex location and determines delta size (Jerolmack, 2009; Ganti et al., 2016a). The avulsion node on some landforms, typically steeper fan-deltas and alluvial fans, is controlled by valley width and slope variations (Blair & McPherson, 1994; Ganti et al., 2014; Hartley et al., 2017), but on lowland deltas avulsion nodes persist on unconfined alluvial plains. The distance from the shoreline to the avulsion node, termed the avulsion length (L_A), typically scales with the backwater length-scale of the river (L_b), that is, the ratio of channel depth (H_c) to bed-slope (S) (i.e., $L_A \sim L_b = \frac{H_c}{S}$) (Figure 1a) (Paola & Mohrig, 1996; Jerolmack & Swenson, 2007; Chatanantavet et al., 2012). The backwater length approximates the distance that sea level influences river flow upstream and can extend for hundreds of kilometers for low-sloping rivers (Lamb et al., 2012).

The Huanghe, China, provides an example where seven consecutive backwater-scaled avulsions occurred before major engineering (Ganti et al., 2014). In addition, abandoned lobes record six Holocene avulsions on the Mississippi that occurred within the backwater zone (Coleman et al., 1998; Chatanantavet et al., 2012), while two avulsions occurred farther upstream (Saucier, 1994; Chamberlain, 2018). Because river avulsions occur infrequently and

are difficult to observe directly, flume experiments and numerical modeling have contributed substantially to our understanding. These modeling studies, however, differ in their explanation for the origin of persistent, backwater-scaled avulsion nodes.

Chatanantavet et al. (2012) hypothesized that avulsion nodes on lowland deltas originate from heightened in channel-bed aggradation in the backwater zone that emerges due to flows of variable discharge. Using quasi-2D morphodynamic simulations, they showed that low flows deposit sediment in the upstream part of the backwater zone and high flows focus erosion and bypass farther downstream, resulting in a persistent peak in net aggradation in the middle of the backwater zone. Constant-discharge simulations, in contrast, yielded quasi-uniform flow and uniform bed-aggradation rates. Chatanantavet et al. (2012) did not simulate avulsions and lobe switching, and the river mouth in their study was unrealistically fixed which prevented riverbed aggradation due to progradation. Nonetheless, subsequent flume experiments that included progradation and natural lobe switching and reactivation supported their hypothesis by showing persistent avulsions about a preferential node at $L_A \sim 0.5L_b$, coinciding with a peak in channel-bed aggradation for an experiment with variable flows (Ganti et al., 2016a; 2016b). In contrast, a comparable constant-discharge experiment did not produce a persistent node, indicating that flow variability is the dominant mechanism to produce backwater-scaled avulsions.

Later numerical modeling studies by Moran et al. (2017) and Ratliff (2017), however, simulated delta growth with river-mouth progradation under a range of relative-sea-level-rise rates and constant-discharge conditions, and found backwater-scaled avulsion nodes despite the lack of flow variability. In their models, a wedge of sediment migrated downstream on a riverbed with an initially uniform slope, and eventually aggradation exceeded an imposed avulsion threshold. Thus, in contrast to experiments (Ganti et al., 2016a; 2016b) and earlier models (Chatanantavet et al., 2012), these studies suggest that backwater-scaled avulsions

can be produced in models with constant water discharge. However, these models invoked a potentially unrealistic riverbed of uniform slope as an initial condition, and measured the potential for avulsion in terms of sediment accumulation thickness relative to the initial topography. In contrast, in natural environments, deltas tend to reoccupy lobes and build over previous fluvio-deltaic deposits. Thus, the assumed initial conditions in these numerical models might affect the emergence of an avulsion node.

Here we aim to elucidate the origin of a preferential avulsion node and unify the contradictory results of previous work. In particular, the model of Chatanantavet et al. (2012) requires flow variability to produce a persistent avulsion node, consistent with available experimental data, but the elimination of river-mouth progradation in their model might have biased their results. In contrast, more recent models (Moran et al., 2017; Ratliff, 2017) can produce persistent avulsion nodes with constant discharge, but they impose an unrealistic initial condition. To address these potentially problematic assumptions, we constructed a quasi-2D numerical model that allows for repeated lobe construction and avulsion such that lobes build on top of one another, thereby minimizing the role of initial topography as the delta evolves. The model also allows for river-mouth progradation. We explored the model behavior over parameter space relevant to natural lowland deltas, including variable flow regimes and relative sea-level rise, to identify the conditions that cause a preferential backwater-scaled avulsion node.

2. Methods

We aimed to isolate the cause of preferential avulsion nodes using a simplified model that captures delta-lobe construction, avulsion and reoccupation, and river-mouth progradation on lowland river deltas. The model does not represent a specific delta. Instead,

the framework is generic and includes a deltaic plain with an imposed number of lobes (Figure 1b).

Following previous work, we modeled each lobe as a coupled river and floodplain of uniform floodplain width (B_f), channel sinuosity (Ω), wash-load ratio (Λ), and bed porosity (λ_p), which is well-described by a quasi-two-dimensional mass-balance framework (Parker, 2004; Parker et al., 2008a; 2008b; Chatanantavet et al. 2012). Sediment mass-balance also incorporates a floodplain representing the active delta lobe extent,

$$\frac{\partial \eta_b}{\partial t} + \sigma = -\frac{(1+\Lambda)\Omega}{(1-\lambda_p)B_f}\frac{\partial B q_t}{\partial x}, \qquad \text{equation 1}$$

where η_b is channel bed elevation relative to sea level, t is time, σ is relative-sea-level-rise rate, x is downstream distance, and q_t is width-averaged flux of total bed-material load. Sediment is transported in a river of width B, and deposited uniformly over the floodplain width B_f (Parker, 2004). We routed water using a quasi-2D backwater equation for water mass and momentum conservation under quasi-steady flow conditions (Chatanantavet et al., 2012),

$$\frac{dH}{dx} = \frac{S - S_f}{1 - Fr^2} + \frac{Fr^2}{1 - Fr^2}\frac{H}{B}\frac{dB}{dx} \qquad \text{equation 2}$$

where H represents the channel depth, S is channel-bed slope, and $S_f = C_f Fr^2$ is friction slope with friction coefficient C_f and Froude number Fr. We assumed uniform channel width and a plume with constant spreading angle offshore (Lamb et al., 2012; Chatanantavet et al, 2012), but unlike previous formulations the plume in our model advances and retreats in concert with the river mouth (Text S1). We routed sediment according to Engelund-Hansen (1967) for total bed-material load,

$$q_t = \sqrt{RgD^3}\,\frac{\alpha}{C_f}\,(\tau^*)^n \qquad \text{equation 3}$$

where R is submerged specific density of sediment, g is gravity, D is the median grain-size of bed material, τ^* is Shields number, and $\alpha = 0.05$ and $n = 2.5$ (Engelund & Hansen, 1967). Equations 2 and 3 adequately describe backwater hydrodynamics and sediment transport of sand-bedded rivers (Lamb et al., 2012; Nittrouer et al., 2012; Chatanantavet et al., 2014).

We approximated deltaic evolution over multiple cycles of lobe-switching using four one-dimensional profiles of predefined width, representing four distinct lobes (Figure 1b-c). Our choice of four lobes is arbitrary, but reasonable based on field observations (Roberts, 1997; Chu et al., 2006) and flume experiments (Reitz et al., 2010; Carlson et al., 2018). One delta lobe was active at a given time (Slingerland & Smith, 2004; Hajek & Edmonds, 2014), and the active lobe evolution was governed by equations 1-3 and solved using finite differences (Text S2). We varied sediment supply at the upstream end with water discharge such that the normal-flow bed slope was held constant, and therefore erosion and deposition were not driven by changes in sediment-supply and water-discharge ratios (Paola, 2000). For the delta front, we used a moving-boundary formulation following Swenson et al. (2000) and others (Text S1). Inactive lobe shapes were unchanged when abandoned, approximating a river-dominated delta where reworking is minimal (Galloway, 1975); however abandoned lobes were partially drowned in cases due to relative sea-level rise.

We used an avulsion criterion given by a critical thickness of aggradation, which we refer to as superelevation ($\Delta\eta$):

$$\Delta\eta(x) \geq H^* H_c \qquad \text{equation 4}$$

in which H_c is the bankfull channel depth and H^* is the avulsion threshold, a dimensionless number that is of order unity (Jerolmack & Mohrig, 2007; Ganti et al., 2014), which we set to $H^* = 0.5$ consistent with field and experimental observations (Mohrig et al., 2000; Ganti et al., 2014; Ganti et al., 2016b). The critical superelevation $\Delta\eta$ may represent the local floodplain (or levee) elevation relative to the distant floodplain or inactive lobes, or the bed

aggradation thickness since the last avulsion (Figure 1c) (Mohrig et al., 2000; Hajek & Wolinsky, 2012; Ganti et al., 2014). In our model the floodplain (η_f) aggrades in concert with the channel bed ($\eta_f = \eta_b + H_c$; Text S1; Figure 1c) and inactive lobes remain unchanged once abandoned, so both explanations hold. We triggered an avulsion when and where the floodplain elevation of the active lobe exceeded the floodplain elevation of the lowest-elevation abandoned lobe ($\eta_{f,abandoned}$), evaluated at the same distance downstream from the trunk channel:

$$\Delta\eta(x) = \begin{cases} \eta_f(x) - \eta_{f,abandoned}(x) & \text{for } x \le x_{m,abandoned} \\ \eta_f(x) - \xi_{sea} & \text{for } x > x_{m,abandoned} \end{cases} \quad \text{equation 5}$$

where $x_{m,abandoned}$ is the stream-wise coordinate of the abandoned-lobe shoreline (Figure 1c). Seaward of the abandoned lobe, superelevation is measured relative to sea level (ξ_{sea}), consistent with assumptions in previous work (Ratliff, 2017). The occurrence of extreme floods and hydraulic connectivity with abandoned channels may also affect the location and timing of any one avulsion (Ganti et al., 2014; Nicholas et al., 2018), but following previous work these effects were neglected in our treatment of multiple avulsion cycles (Jerolmack & Paola, 2007; Hajek & Wolinsky, 2012).

After an avulsion, the river was routed to the lowest abandoned lobe by joining the bed profile of the active channel upstream of the avulsion site (the trunk channel) with the bed profile of the new flow path downstream (the daughter channel; Text S2). This process mimics the tendency of rivers to select steeper paths, fill in topographic lows (Slingerland & Smith, 2004; Straub et al., 2009), and to reoccupy previously abandoned channels (Reitz & Jerolmack, 2012). After establishing the new flow path, lobe construction (equations 1-3) and avulsion setup (equation 4) began anew.

At the start of each model run, the initial state of the riverbed was assumed planar with a uniform downstream slope set to the transport slope for normal flow, similar to

previous studies (Chatanantavet et al., 2012; Moran et al., 2017, Ratliff, 2017). However, due to the imposed number of lobes, after four avulsion cycles the river was forced to reoccupy lobes that were previously active. Thus, unlike previous work, the effect of the initial conditions were minimized after the fourth avulsion cycle.

For variable-discharge simulations, we implemented flow variability using a log-normal distribution of normal-flow depths (Text S3). The distribution is defined by the bankfull-exceedance probability F_{bf}, which describes the frequency of overbank flows relative to all possible flows, and the coefficient of variation CV, which describes the magnitude of low flows and high flows relative to the average flow. We randomly sampled the distribution with a characteristic flow-event duration (T_e) (Figure S1). Gauge data of monthly-mean stage height ($T_e = 1$ month) from several lowland rivers show $F_{bf} \sim 5 - 20\%$ and $CV \sim 0.2 - 0.9$ (Table S1; Ganti et al. 2014).

Our simulations explore how deltaic avulsion patterns respond to variable river discharge, relative sea-level rise, and initial topography by systematically varying the discharge and sea-level parameters for a base case characteristic of large, low-sloping deltas. We non-dimensionalized the model so that it can be applied to a wide range of river conditions (Text S4). The model is governed by nine input dimensionless parameters: bankfull Froude number in the normal-flow reach ($Fr_{n,bf}$), bankfull Shields number in the normal-flow reach ($\tau^*_{n,bf}$), friction factor (C_f), offshore basin floor depth normalized by bankfull depth (H_b^*), time normalized by the channel adjustment timescale ($t^* \sim \frac{tq_t}{L_b H_c}$), a dimensionless rate of relative sea-level rise ($\sigma^* \sim \frac{\sigma L_b}{q_t}$), and the flow variability parameters (F_{bf}, CV, T_e^*; Text S3), where $T_e^* = \frac{T_e q_t}{L_b H_c}$ is a dimensionless flow duration. In all simulations presented here, we assumed constant values typical of large sand-bedded rivers where $Fr_{n,bf} = 0.17$, $\tau^*_{n,bf} = 1$, $C_f = 0.005$, $H_b^* = 2$ (Table S1), and changed only flow variability

parameters (F_{bf}, CV, and T_e^*) and relative sea-level rise (σ^*). Model sensitivity to the other parameters is discussed in Text S6. For each set of dimensionless parameters, simulations proceeded until thirteen avulsions occurred, which was sufficient to capture trends in avulsion location (Text S4).

3. Avulsion nodes originating from initial conditions and flow variability

We first considered a scenario of constant river discharge equal to the bankfull condition and constant relative sea level ($\boldsymbol{F_{bf} = 1, CV = 0, \sigma^* = 0}$), with other model parameters set to the base case. During the first four avulsion cycles, the delta built lobes on the initial surface, which was a plane with a uniform seaward slope. The first avulsion occurred after 1.8 normalized time ($\boldsymbol{\Delta t^* = 1.8}$), equivalent to 9-720 years for a range of parameters typical of natural deltas (Table S1; Text S4), with an avulsion length equal to $\boldsymbol{0.78L_b}$ ($\boldsymbol{L_A^* = 0.78}$) (Figure 2a). Avulsion lengths were similar for the second, third, and fourth avulsions ($\boldsymbol{L_A^* = 0.74, 0.68, 0.98, \text{respectively}}$). In contrast, after avulsion cycle four the constant-discharge delta built upon previously abandoned delta lobes and did not produce a backwater-scaled avulsion node. Normalized avulsion lengths varied considerably for these later avulsions ($\boldsymbol{L_A^* = 0.79 - 8.3}$), and when avulsions occurred a reach of $\boldsymbol{3 - 5L_b}$ was within 10% of the avulsion threshold, indicating no dominant avulsion location.

The consistent avulsion length during the first four avulsion cycles was a consequence of the assumed initial bed topography, and not due to backwater hydrodynamics. Delta front progradation led to channel aggradation and a quasi-steady concave-up bed elevation profile (Muto & Swenson, 2005; Bijkerk et al., 2016), in contrast to the uniform-slope bed profiles that were assumed for all lobes as initial conditions. Differencing the concave-up active lobe profile from the uniform-slope of the lowest inactive (and yet to be active) lobe profile

resulted in a systematic downstream increase in superelevation (Figure 2b). Therefore, avulsions occurred at the farthest downstream location that was allowed, where superelevation was greatest, equivalent to the shoreline location on the inactive lobe of lowest elevation. Seaward of the inactive-lobe shoreline, avulsions did not occur because the active lobe elevation approached sea level and thus superelevation approached zero (Equation 5). Avulsions that occurred at the shoreline of abandoned lobes necessarily scaled with the backwater length due to geometry; lobes prograded a unit fraction of the backwater length-scale before avulsing (i.e., the lobe progradation distance $\boldsymbol{D}$ scales as $\boldsymbol{D \approx H^{*}H_{c}/S \approx H^{*}L_{b}}$; Ganti et al., 2014).

After avulsion cycles 1-4 in the constant-discharge model, the delta completely reworked its initial uniform slope and superelevation therefore was assessed by comparing the active lobe to previously occupied lobes, rather than to the planar initial surface. River profiles in these later avulsion cycles prograded with a quasi-steady and self-similar shape, causing nearly uniform deposition and a similar likelihood of avulsions everywhere, including far outside of the backwater zone (Figure 2c). Thus, avulsion locations and their apparent scaling with the backwater length in cycles 1-4 were a geometric artifact resulting from the assumed initial bed topography. Four avulsions were required to rework the initial condition because four delta lobes were imposed (Figure 1A; Text S6). In absence of the uniform-slope initial condition, constant-discharge conditions did not produce a persistent backwater-scaled avulsion node.

Next, we considered a model run identical to the constant-discharge case but with variable discharge, using $\boldsymbol{CV = 0.53,\ F_{bf} = 0.05, \text{and } T_{e}^{*} = 0.001}$, which is typical of lowland rivers (Table S1). In this case, we observed a preferential avulsion node corresponding to an avulsion length nearly equal to the backwater length-scale, $\boldsymbol{L_{A}^{*} = L_{A}/L_{b} \sim 1}$ (Figure 2d) which persisted through many avulsion cycles even after there was no

longer an influence from the planar initial surface (Figure 2e-f). Consistent with previous studies (Lamb et al., 2012; Chatanantavet et al., 2012; Ganti et al., 2016a), periods of low flow had enhanced deposition due to spatial deceleration through the backwater zone and high flows eroded the downstream-most reach, resulting in a spatial peak in deposition rate midway through the backwater zone when averaged over many flow events. The avulsion node was coincident with the location of maximum deposition rate, and only a short reach ($< \mathbf{0.4}\boldsymbol{L_b}$) was within 10% of the threshold at the time of an avulsion. Outliers are due to major avulsions that shifted the avulsion node downstream once the four lateral lobes were built, causing trunk channel aggradation and overall shoreline progradation (Text S5; Figure S2).

4. Necessary degree of flow variability

Given the importance of variable flows in controlling avulsion location for deltas that lack uniform bed slopes as initial conditions, we quantified how much flow variability is necessary to drive a preferential avulsion node. We ran 21 numerical experiments to systematically vary the coefficient of flow variation ($\boldsymbol{CV}$), bankfull-exceedance probability ($\boldsymbol{F_{bf}}$), and dimensionless flow duration ($\boldsymbol{T_e^*}$) within a parameter space that represents many natural rivers (Table S1). For each model run we changed one of these parameters and held all other parameters to base-case values. We focused our analysis on cycles 5-13 that were not affected by the initial uniform bed slope.

Isolation of the coefficient of variation ($\boldsymbol{CV}$) reveals that there is an intermediate range $\mathbf{0.1} < \boldsymbol{CV} < \mathbf{0.6}$ where modeled deltas preferentially avulsed within the upstream half of the backwater zone (Figure 3a). Similarly, avulsions occurred at a preferential node so long as less than 5% of flows exceeded bankfull ($\boldsymbol{F_{bf}} < \mathbf{0.05}$; **Figure 3b**) and that the duration of flow events was less than 10% of the reach-filling timescale ($\boldsymbol{T_e^*} <$

$\mathbf{0.1}$; **Figure 3c**). The conditions needed for a preferential avulsion node predicted by the model are common for natural lowland rivers (Table S1) and correspond to a state of continuous riverbed adjustment, where the scours cut by large floods are partially filled during intervening low flows. Continuous riverbed adjustment is necessary for persistent backwater effects (Chatanantavet et al., 2014) and in our model resulted in broad convex-up portions of the long profile when averaged over many flood events (Figure S3). Under milder flow regimes ($\boldsymbol{CV < 0.1}$) and longer flow durations ($\boldsymbol{T_e^* > 0.1}$) the riverbed fully adjusted to normal-flow conditions, resulting in uniform aggradation rates without a preferential avulsion location similar to the constant-discharge scenario. Flashier flow regimes ($\boldsymbol{CV > 0.6}$) and high probabilities of bankfull exceedance ($\boldsymbol{F_{bf} > 0.05}$) also lacked a preferred avulsion node, as the riverbed adjusted to normal-flow conditions associated with large floods.

5. Avulsion nodes originating from relative sea-level rise

In previous sections, the dimensionless relative-sea-level-rise rate was set to zero to isolate the initial conditions and flow variability. To relax this assumption, we varied the dimensionless relative-sea-level-rise rate across a range that encompasses many modern deltas ($\boldsymbol{\sigma^* = 10^{-3} - 10^{0}}$) under constant-discharge (Figure 3d) and variable-discharge (Figure 3e) conditions, with other parameters identical to the base case (Table S1). Similar to the scenario of $\boldsymbol{\sigma^* = 0}$, constant-discharge deltas with $\boldsymbol{\sigma^* = 10^{-3} - 10^{-1}}$ did not have a preferential node, whereas all variable-discharge cases had a preferential avulsion node with $\boldsymbol{L_A/L_b \sim 1}$. Thus, relative sea-level rise at moderate rates common to modern deltas did not significantly affect avulsion node occurrence (Figure 3d-e). However, at very high rise rates ($\boldsymbol{\sigma^* > 10^{-1}}$) the river mouth retreated upstream, forcing a strong downstream increase in

deposition. Thus, for $\boldsymbol{\sigma^* > 10^{-1}}$ the downstream increase in aggradation resulted in avulsion locations that coincided with the shoreline of the lowest-elevation inactive lobe, which scaled with the backwater length for the same geometric reasons as in the cases with planar initial conditions (Figure S4).

6. Discussion and Conclusions

Our results reconcile previous work by showing that variable flow regimes are necessary to produce backwater-scaled avulsion nodes on lowland deltas. Our finding is consistent with experiments that isolated the role of flow variability (Ganti et al., 2016a) on deltas that experienced continuous lobe growth, abandonment and reoccupation. A certain amount of flow variability ($\boldsymbol{0.1 < CV < 0.6,\ F_{bf} < 0.05,\ T_e^* < 0.1}$) is necessary to produce persistent backwater effects so that the riverbed is in a continual state of morphodynamic adjustment (Chatanantavet et al., 2014). These conditions are common to natural rivers (Table 1). Continual bed adjustment from floods in our model produced very broad, low-relief upward convexities in the riverbed in the backwater zone (Figure 2e-f; Figure S3), consistent with the bed topography of the lower 200-700 km of the Mississippi (Harmar, 2004; Nittrouer et al., 2012; Figure S5), which may be a topographic signature of backwater-mediated avulsions in other rivers.

In contrast, constant-discharge numerical experiments tend towards a graded state without strong backwater effects or a preferential node location. Our results suggest that previous numerical models that lacked variable discharges and produced backwater-scaled avulsions (Moran et al., 2017; Ratliff, 2017) were likely affected by initial conditions of uniformly sloped initial surfaces. A backwater-scaled avulsion node under these conditions is a geometric consequence of assessing superelevation of a prograding channel or lobe relative

to a planar seaward-sloping landscape. For similar reasons, relative sea-level rise can also cause persistent avulsion nodes under constant discharge conditions, but only under high rise rates that cause marine transgression. In these cases, avulsions occur at the most downstream location allowed – near the inactive-lobe shoreline, which was $\sim \boldsymbol{L_b}$ upstream of the active river mouth at the time of avulsion due to the geometry of lobe progradation. Although the simulations of Chatanantavet et al. (2012) also had an initial uniform bed slope and relative sea-level rise, they did not produce a persistent avulsion node under constant-discharge conditions because the model lacked river-mouth progradation.

In a sensitivity analysis, we found that changing other model parameters does not affect our results on the origin of preferred avulsion node (Text S6). Larger avulsion thresholds, $\boldsymbol{H}^*$, cause avulsions to occur farther upstream, but do not change the overall results (Figure S6). Likewise, the number of imposed delta lobes affects the number of avulsion cycles that are affected by the initial conditions, and the frequency of trunk-channel-filling avulsions (Text S5), but does not affect the origin of a preferential avulsion node.

Our variable-discharge simulations produced avulsion lengths within a factor of two of the backwater length-scale, similar to the distribution of avulsion lengths on the Huanghe (Ganti et al., 2014) and Mississippi (Coleman et al., 1998; Chatanantavet et al., 2012). Following four lateral avulsions that occupied the available prograding lobes, the avulsion node in our model shifted downstream in tandem with net shoreline progradation, as has been documented on the Huanghe (Ganti et al., 2014) and in flume experiments (Ganti et al., 2016a). Our model also produced outliers in the avulsion-length distribution, where deltas with a backwater-scaled avulsion node sometimes have avulsions much farther upstream, similar to the Mississippi (Chamberlain et al., 2018). These larger-scale avulsions occurred in our model near the time when the avulsion node shifted downstream; once a full set of lateral

avulsions occurred, the trunk channel upstream of the avulsion node must aggrade to allow continued net progradation (Text S5).

Avulsion node locations could be different when channels reoccupy topographically dissimilar lobes (e.g., the Danube; Giosan et al., 2005), cut new channels in the floodplain (Hajek & Edmonds, 2014), or where lobes have been modified by marine processes (e.g., the Red River; Mathers & Zalasiewicz, 1999). However, when channels build upon topographically similar abandoned delta-lobe topography, which is a common scenario, a backwater-scaled avulsion node emerges when flow variability is sufficient to cause a peak in aggradation within the backwater zone. Thus, changing flow regimes due to climate or built infrastructure may affect flood hazards and wetland sustainability by shifting the location of future avulsions.

Acknowledgments, Samples, and Data

We acknowledge National Science Foundation grant EAR 1427262 and the Resnick Sustainability Institute at Caltech for support. We thank Vamsi Ganti, Gail Kineke, Ben

Hobbs, Hongbo Ma, Brandee Carlson, Kensuke Naito, and Lisa Kumpf for insightful discussions, and Elizabeth Hajek and Wonsuck Kim for constructive reviews.

Data are available at: *http://sead-published.ncsa.illinois.edu/seadrepository/api/researchobjects/urn:uuid:5c37c889e4b0a8e144f6565f*

Code is available at: https://github.com/achadwick2323/Origin-of-a-preferential-avulsion-node-on-lowland-river-deltas

References

Andrews, E. D. (1980). Effective and bankfull discharges of streams in the Yampa River basin, Colorado and Wyoming. *Journal of Hydrology*, *46*(3-4), 311-330.

Baumanis, C., & Kim, W. (2018). Reverse migration of lithofacies boundaries and shoreline in response to sea-level rise. *Basin Research*, *30*, 89-100.

Bijkerk, J. F., Eggenhuisen, J. T., Kane, I. A., Meijer, N., Waters, C. N., Wignall, P. B., & McCaffrey, W. D. (2016). Fluvio-marine sediment partitioning as a function of basin water depth. *Journal of Sedimentary Research*, *86*(3), 217-235.

Blair, T. C., & McPherson, J. G. (1994). Alluvial fans and their natural distinction from rivers based on morphology, hydraulic processes, sedimentary processes, and facies assemblages. *Journal of sedimentary research*, *64*(3a), 450-489.

Borland, W. M. (1971). Reservoir sedimentation. River mechanics, 2, 29-1.

Carlson, B., Piliouras, A., Muto, T., & Kim, W. (2018). Control of Basin Water Depth On Channel Morphology and Autogenic Timescales in Deltaic Systems. *Journal of Sedimentary Research*, *88*(9), 1026-1039.

Chamberlain, E. L., Törnqvist, T. E., Shen, Z., Mauz, B., & Wallinga, J. (2018). Anatomy of Mississippi Delta growth and its implications for coastal restoration. *Science advances*, *4*(4), eaar4740.

Chatanantavet, P., Lamb, M. P., & Nittrouer, J. A. (2012). Backwater controls of avulsion location on deltas. *Geophysical Research Letters*, *39*(1).

Chatanantavet, P., & Lamb, M. P. (2014). Sediment transport and topographic evolution of a coupled river and river plume system: An experimental and numerical study. *Journal of Geophysical Research: Earth Surface*, *119*(6), 1263-1282.

Chu, Z. X., Sun, X. G., Zhai, S. K., & Xu, K. H. (2006). Changing pattern of accretion/erosion of the modern Yellow River (Huanghe) subaerial delta, China: Based on remote sensing images. *Marine Geology*, *227*(1-2), 13-30.

Church, M. (2006). Bed material transport and the morphology of alluvial river channels. *Annu. Rev. Earth Planet. Sci.*, *34*, 325-354.

Coleman, J. M., Roberts, H. H., & Stone, G. W. (1998). Mississippi River delta: an overview. Journal of Coastal Research, 14(3).

Dade, W. B., & Friend, P. F. (1998). Grain-size, sediment-transport regime, and channel slope in alluvial rivers. *The Journal of Geology*, *106*(6), 661-676.

Edmonds, D. A., Hoyal, D. C., Sheets, B. A., & Slingerland, R. L. (2009). Predicting delta avulsions: Implications for coastal wetland restoration. *Geology*, *37*(8), 759-762.

Einstein, H. A. (1950), The bed-load function for sediment transportation in open channel flows, Technical Bulletin 1026, U.S. Dept. of the Army, Soil Conservation Service.

Engelund, F., & Hansen, E. (1967). A monograph on sediment transport in alluvial streams. *Technical University of Denmark 0stervoldgade 10, Copenhagen K.*

Fernandes, A. M., Törnqvist, T. E., Straub, K. M., & Mohrig, D. (2016). Connecting the backwater hydraulics of coastal rivers to fluvio-deltaic sedimentology and stratigraphy. *Geology*, *44*(12), 979-982.

Galloway, W. (1975). Process framework for describing the morphologic and stratigraphic evolution of deltaic depositional systems. *Deltas: Models for Exploration*.

Galloway, W. E. (1989). Genetic stratigraphic sequences in basin analysis I: architecture and genesis of flooding-surface bounded depositional units. *AAPG bulletin*, *73*(2), 125-142.

Ganti, V., Chu, Z., Lamb, M. P., Nittrouer, J. A., & Parker, G. (2014). Testing morphodynamic controls on the location and frequency of river avulsions on fans versus deltas: Huanghe (Yellow River), China. *Geophysical Research Letters*, *41*(22), 7882-7890.

Ganti, V., Chadwick, A. J., Hassenruck-Gudipati, H. J., Fuller, B. M., & Lamb, M. P. (2016). Experimental river delta size set by multiple floods and backwater hydrodynamics. *Science advances*, *2*(5), e1501768.

Ganti, V., Chadwick, A. J., Hassenruck-Gudipati, H. J., & Lamb, M. P. (2016). Avulsion cycles and their stratigraphic signature on an experimental backwater-controlled delta. *Journal of Geophysical Research: Earth Surface*, *121*(9), 1651-1675.

Giosan, L., Donnelly, J. P., Vespremeanu, E., Bhattacharya, J. P., Olariu, C., & Buonaiuto, F. S. (2005). River delta morphodynamics: Examples from the Danube delta.

Hajek, E. A., & Edmonds, D. A. (2014). Is river avulsion style controlled by floodplain morphodynamics?. *Geology*, *42*(3), 199-202.

Hajek, E. A., & Wolinsky, M. A. (2012). Simplified process modeling of river avulsion and alluvial architecture: connecting models and field data. Sedimentary Geology, 257, 1-30.

Harmar, O. P. (2004). *Morphological and process dynamics of the Lower Mississippi River* (Doctoral dissertation, University of Nottingham).

Hartley, A. J., Weissmann, G. S., & Scuderi, L. (2017). Controls on the apex location of large deltas. *Journal of the Geological Society*, *174*(1), 10-13.

Hotchkiss, R. H., & Parker, G. (1991). Shock fitting of aggradational profiles due to backwater. *Journal of Hydraulic Engineering*, *117*(9), 1129-1144.

Jerolmack, D. J., & Mohrig, D. (2007). Conditions for branching in depositional rivers. *Geology*, *35*(5), 463-466.

Jerolmack, D. J., & Paola, C. (2007). Complexity in a cellular model of river avulsion. Geomorphology, 91(3-4), 259-270.

Jerolmack, D. J., & Swenson, J. B. (2007). Scaling relationships and evolution of distributary networks on wave-influenced deltas. *Geophysical Research Letters*, *34*(23).

Jerolmack, D. J. (2009). Conceptual framework for assessing the response of delta channel networks to Holocene sea level rise. *Quaternary Science Reviews*, *28*(17), 1786-1800.

Kidder, T. R., & Liu, H. (2017). Bridging theoretical gaps in geoarchaeology: Archaeology, geoarchaeology, and history in the Yellow River valley, China. *Archaeological and Anthropological Sciences*, *9*(8), 1585-1602.

Kim, W., Paola, C., Voller, V. R., & Swenson, J. B. (2006). Experimental measurement of the relative importance of controls on shoreline migration. *Journal of Sedimentary Research*, *76*(2), 270-283.

Kostic, S., & Parker, G. (2003). Progradational sand-mud deltas in lakes and reservoirs. Part 1. Theory and numerical modeling. *Journal of Hydraulic Research*, *41*(2), 127-140.

Lague, D., Hovius, N., & Davy, P. (2005). Discharge, discharge variability, and the bedrock channel profile. Journal of Geophysical Research: Earth Surface, 110(F4).

Lamb, M. P., Nittrouer, J. A., Mohrig, D., & Shaw, J. (2012). Backwater and river plume controls on scour upstream of river mouths: Implications for fluvio-deltaic morphodynamics. *Journal of Geophysical Research: Earth Surface*, *117*(F1).

Langbein, W. B., & Leopold, L. B. (1964). Quasi-equilibrium states in channel morphology. *American Journal of Science*, *262*(6), 782-794.

LeBoutillier, D. W., & Waylen, P. R. (1993). A stochastic model of flow duration curves. *Water Resources Research*, *29*(10), 3535-3541.

Liang, M., Van Dyk, C., & Passalacqua, P. (2016). Quantifying the patterns and dynamics of river deltas under conditions of steady forcing and relative sea level rise. *Journal of Geophysical Research: Earth Surface*, *121*(2), 465-496.

Maselli, V., Pellegrini, C., Del Bianco, F., Mercorella, A., Nones, M., Crose, L., Guerrero, M., & Nittrouer, J. A. (2018). River Morphodynamic Evolution Under Dam-Induced Backwater: An Example from the Po River (Italy). *Journal of Sedimentary Research*, 88(10), 1190-1204.

Mathers, S., & Zalasiewicz, J. (1999). Holocene sedimentary architecture of the Red River delta, Vietnam. *Journal of Coastal Research*, 314-325.

Milliman, J. D., & Syvitski, J. P. (1992). Geomorphic/tectonic control of sediment discharge to the ocean: the importance of small mountainous rivers. *The Journal of Geology*, *100*(5), 525-544.

Mohrig, D., Heller, P. L., Paola, C., & Lyons, W. J. (2000). Interpreting avulsion process from ancient alluvial sequences: Guadalope-Matarranya system (northern Spain) and

Wasatch Formation (western Colorado). *Geological Society of America Bulletin*, *112*(12), 1787-1803.

Moran, K. E., Nittrouer, J. A., Perillo, M. M., Lorenzo- Trueba, J., & Anderson, J. B. (2017). Morphodynamic modeling of fluvial channel fill and avulsion time scales during early Holocene transgression, as substantiated by the incised valley stratigraphy of the Trinity River, Texas. *Journal of Geophysical Research: Earth Surface*, *122*(1), 215-234.

Muto, T., & Steel, R. J. (1997). Principles of regression and transgression: the nature of the interplay between accommodation and sediment supply: perspectives. *Journal of Sedimentary Research*, *67*(6).

Muto, T., & Steel, R. J. (2002). Role of autoretreat and A/S changes in the understanding of deltaic shoreline trajectory: a semi- quantitative approach. *Basin Research*, *14*(3), 303-318.

Muto, T., & Swenson, J. B. (2005). Large-scale fluvial grade as a nonequilibrium state in linked depositional systems: Theory and experiment. *Journal of Geophysical Research: Earth Surface*, *110*(F3).

Nicholas, A. P., Aalto, R. E., Sambrook Smith, G. H., & Schwendel, A. C. (2018). Hydrodynamic controls on alluvial ridge construction and avulsion likelihood in meandering river floodplains. *Geology*.

Nittrouer, J. A., Mohrig, D., Allison, M. A., & Peyret, A. P. B. (2011). The lowermost Mississippi River: a mixed bedrock- alluvial channel. *Sedimentology*, *58*(7), 1914-1934.

Nittrouer, J. A., Shaw, J., Lamb, M. P., & Mohrig, D. (2012). Spatial and temporal trends for water-flow velocity and bed-material sediment transport in the lower Mississippi River. *Bulletin*, *124*(3-4), 400-414.

Pang, J. Z., & Si, S. H. (1979). Evolution of the Yellow River mouth: I. Historical shifts. *Oceonologia et Limnologia Sinica*, *10*(2), 136-141.

Paola, C. (2000). Quantitative models of sedimentary basin filling. *Sedimentology*, *47*(s1), 121-178.

Paola, C., & Mohrig, D. (1996). Palaeohydraulics revisited: palaeoslope estimation in coarse-grained braided rivers. *Basin Research*, *8*(3), 243-254.

Paola, C., Twilley, R. R., Edmonds, D. A., Kim, W., Mohrig, D., Parker, G., Viparelli, E., & Voller, V. R. (2011). Natural processes in delta restoration: Application to the Mississippi Delta. *Annual Review of Marine Science*, *3*, 67-91.

Parker, G. (1979), Hydraulic geometry of active gravel rivers, J. Hydraul. Eng., 105(9), 1185–1201.

Parker, G. (2004). 1D sediment transport morphodynamics with applications to rivers and turbidity currents. *E-book available at Gary Parker's Morphodynamics Web Page, last update April*, *13*, 2006.

Parker, G., Muto, T., Akamatsu, Y., Dietrich, W. E., & Lauer, J. (2008). Unravelling the conundrum of river response to rising sea-level from laboratory to field. Part I: Laboratory experiments. *Sedimentology*, *55*(6), 1643-1655.

Parker, G., Muto, T., Akamatsu, Y., Dietrich, W. E., & Wesley Lauer, J. (2008). Unravelling the conundrum of river response to rising sea-level from laboratory to field. Part II. The Fly–Strickland River system, Papua New Guinea. *Sedimentology*, *55*(6), 1657-1686.

Parker, G., Wilcock, P. R., Paola, C., Dietrich, W. E., & Pitlick, J. (2007). Physical basis for quasi-universal relations describing bankfull hydraulic geometry of single-thread gravel bed rivers. *Journal of Geophysical Research: Earth Surface*, *112*(F4).

Ratliff, K. M. (2017). *From the River to the Sea: Modeling Coastal River, Wetland, and Shoreline Dynamics* (Doctoral dissertation).

Reitz, M. D., Jerolmack, D. J., & Swenson, J. B. (2010). Flooding and flow path selection on alluvial fans and deltas. *Geophysical Research Letters*, *37*(6).

Reitz, M. D., & Jerolmack, D. J. (2012). Experimental alluvial fan evolution: Channel dynamics, slope controls, and shoreline growth. *Journal of Geophysical Research: Earth Surface*, *117*(F2).

Richards, K., Brasington, J., & Hughes, F. (2002). Geomorphic dynamics of floodplains: ecological implications and a potential modelling strategy. *Freshwater Biology*, *47*(4), 559-579.

Richards, K., Brasington, J., & Hughes, F. (2002). Geomorphic dynamics of floodplains: ecological implications and a potential modelling strategy. *Freshwater Biology*, *47*(4), 559-579.

Roberts, H. H. (1997). Dynamic changes of the Holocene Mississippi River delta plain: the delta cycle. *Journal of Coastal Research*, 605-627.

Saucier, R. T. (1994). Geomorphology and quaternary geologic history of the Lower Mississippi Valley (Vol. 1). US Army Engineer Waterways Experiment Station.

Slingerland, R., & Smith, N. D. (2004). River avulsions and their deposits. *Annu. Rev. Earth Planet. Sci.*, *32*, 257-285.

Soong, T. W., & Zhao, Y. (1994). The flood and sediment characteristics of the Lower Yellow River in China. *Water International*, *19*(3), 129-137.

Stedinger, J. R., Vogel, R. M., & Foufoula-Georgiou, E. (1993). Frequency analysis of extreme events, Chapter 18 in Handbook of Hydrology, edited by DR Maidment.

Straub, K. M., Paola, C., Mohrig, D., Wolinsky, M. A., & George, T. (2009). Compensational stacking of channelized sedimentary deposits. *Journal of Sedimentary Research*, *79*(9), 673-688.

Sturm, T. W. (2010). *Open channel hydraulics*. New York: McGraw-Hill.

Swenson, J. B., Voller, V. R., Paola, C., Parker, G., & Marr, J. G. (2000). Fluvio-deltaic sedimentation: A generalized Stefan problem. *European Journal of Applied Mathematics*, *11*(5), 433-452.

Syvitski, J. P., Kettner, A. J., Overeem, I., Hutton, E. W., Hannon, M. T., Brakenridge, G. R., ... & Nicholls, R. J. (2009). Sinking deltas due to human activities. *Nature Geoscience*, *2*(10), 681.

Syvitski, J. P., & Saito, Y. (2007). Morphodynamics of deltas under the influence of humans. *Global and Planetary Change*, *57*(3-4), 261-282.

Venditti, J. G., & Church, M. (2014). Morphology and controls on the position of a gravel-sand transition: Fraser River, British Columbia. *Journal of Geophysical Research: Earth Surface*, *119*(9), 1959-1976.

Wolman, M. G., and J. P. Miller (1960), Magnitude and frequency of forces in geomorphic processes, J. Geol., 68, 54–74, doi:10.1086/626637

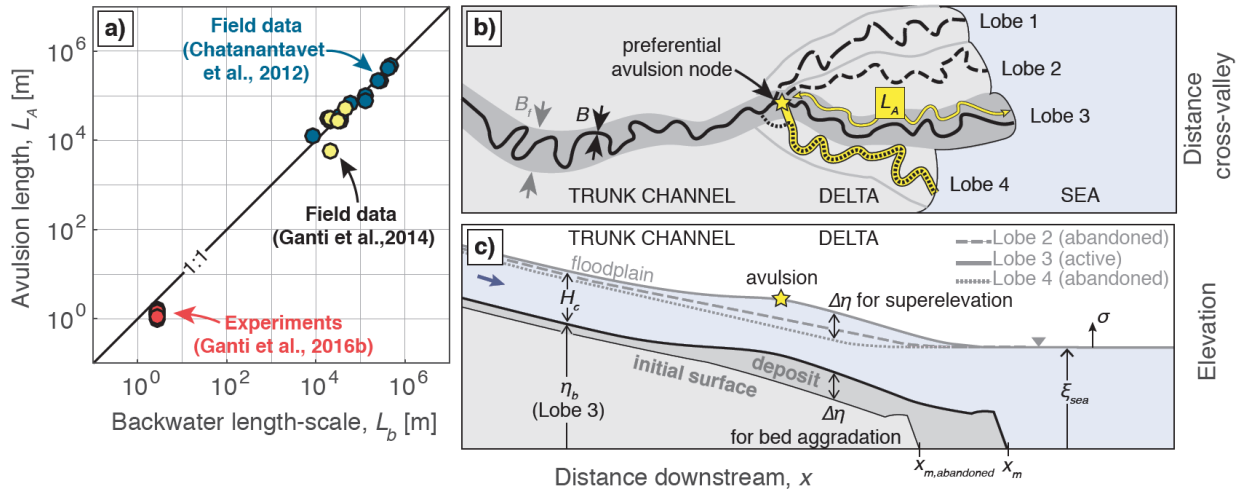

Figure 1) a) Correlation between avulsion length ($\boldsymbol{L_A}$) and backwater length ($\boldsymbol{L_b}$) from lowland river deltas and backwater-influenced experiments b) Planview schematic. Black solid lines are active channel of width $\boldsymbol{B}$ within a floodplain/lobe of width $\boldsymbol{B_f}$ (lobe 3). Broken lines are abandoned channels. After an avulsion, abandoned lobe 4 is reoccupied and its profile is joined with trunk channel at avulsion node (yellow star). c) Cross-section schematic, showing channel aggradation and floodplain superelevation of the active lobe (lobe 3) relative to the lowest abandoned lobe (lobe 4).

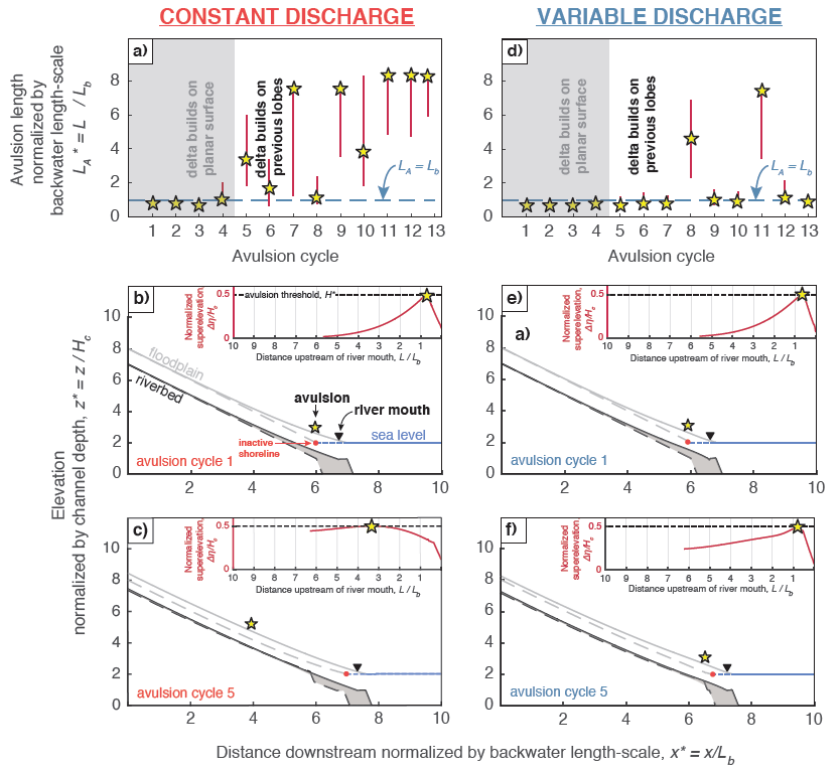

Figure 2) Model results for avulsion length through time over thirteen avulsion cycles under constant discharge (a) and variable discharge (d) with parameters set to base case $\left(\boldsymbol{Fr_{n,bf}} = \mathbf{0.17},\ \boldsymbol{\tau^{*}_{n,bf}} = \mathbf{1},\ \boldsymbol{C_f} = \mathbf{0.005}, \boldsymbol{H^{*}_{b}} = \mathbf{2}\right)$. Red error bars indicate portion of reach within 10% of threshold superelevation necessary for avulsion. Outliers in cycles 8 and 11 of the variable-discharge case are due to transient long-profile adjustment following major avulsions (cycles 7 and 10) that shift the avulsion node seaward and aggrade the trunk channel (Text S5). Results for channel long-profile under constant-discharge conditions (b-c) and variable flows (e-f) for two example avulsion cycles affected (cycle 1) and unaffected (cycle 5) by initial conditions. Black lines are riverbed profile at start (dashed) and end (solid) of an avulsion cycle. Floodplain profiles of active lobe (gray solid line) and lowest inactive lobe (gray dashed line) are used to calculate superelevation (see inset). Downstream of inactive-lobe shoreline location (red circle), floodplain superelevation is measured relative to sea level. Black triangles are river mouth at end of the avulsion cycle. Yellow stars show avulsion location. Delta progradation extended model domain length by $\sim\boldsymbol{4L_b}$ over thirteen cycles, leading to an increase in maximum possible avulsion length.

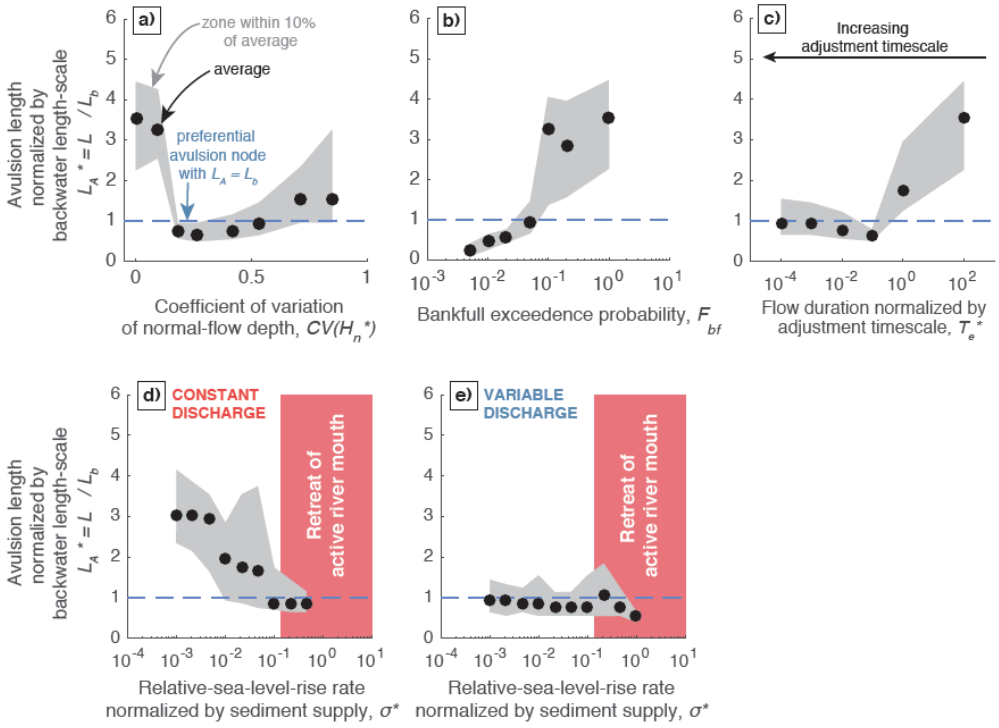

Figure 3) Model results for avulsion length with changing flow variability parameters: $\boldsymbol{CV}$ (a), $\boldsymbol{F_{bf}}$ (b), and $\boldsymbol{T_e^*}$(c), as well as variation of relative-sea-level-rise rate $\boldsymbol{\sigma^*}$ under constant discharge (d) and variable discharge (e). Black circles show avulsion locations averaged over cycles not influenced by initial conditions (cycles 5-13), and gray shaded areas denote the average reach within 10% of avulsion threshold at times of avulsion.